Differential Effects of Caveolin-1 and -2 Knockdown on Aqueous Outflow and Altered Extracellular Matrix Turnover in Caveolin-Silenced Trabecular Meshwork Cells

Mini Aga, John M. Bradley, Rohan Wanchu, Yong-feng Yang, Ted S. Acott, and Kate E. Keller

Casey Eye Institute, Oregon Health & Science University, Portland, Oregon, United States

Correspondence: Kate E. Keller, Casey Eye Institute, Oregon Health & Science University, 3181 SW Sam Jackson Park Road, Portland, OR 97239, USA; gregorka@ohsu.edu.

Submitted: April 4, 2014
Accepted: July 27, 2014

Citation: Aga M, Bradley JM, Wanchu R, Yang Y-F, Acott TS, Keller KE. Differential effects of caveolin-1 and -2 knockdown on aqueous outflow and altered extracellular matrix turnover in caveolin-silenced trabecular meshwork cells. *Invest Ophthalmol Vis Sci*. 2014;55:5497–5509. DOI:10.1167/iovs.14-14519

Purpose. A single nucleotide polymorphism (SNP) identified between caveolin-1 (CAV1) and caveolin-2 (CAV2) on chromosome 7 is associated with glaucoma. One function of CAVs is endocytosis and recycling of extracellular matrix (ECM) components. Here, we generated CAV-silencing lentivirus to evaluate the effects on ECM turnover by trabecular meshwork (TM) cells and to measure the effect on outflow facility in anterior segment perfusion culture.

Methods. Short hairpin CAV1 and CAV2 silencing and control lentivirus were generated, characterized, and applied to anterior segments in perfusion culture. Colocalization of CAVs with various ECM molecules in TM cells was investigated using immunofluorescence and confocal microscopy. Western immunoblotting and fluorogenic-based enzyme activity assays were used to investigate ECM protein levels and degradation, respectively.

Results. Endogenous CAVs colocalized with cortactin at podosome- or invadopodia-like structures (PILS), which are areas of focal ECM degradation. In perfusion culture, outflow rates increased significantly in CAV1-silenced anterior segments, whereas outflow significantly decreased in CAV2-silenced anterior segments. Matrix metalloproteinase (MMP)2 and MMP14, and a disintegrin and metalloproteinase with thrombospondin motifs-4 (ADAMTS4) colocalized with both CAVs in TM cells. Protein levels and enzyme activities of MMP/ADAMTS4, fibronectin protein levels, actin stress fibers, and α-smooth muscle actin were all increased in CAV-silenced cells.

Conclusions. Caveolin-mediated endocytosis is one mechanism by which TM cells can alter the physiological catabolism of ECM in order to change the composition of the outflow channels in the TM to regulate aqueous outflow resistance. Dysregulation of CAV function could contribute to the pathological changes in ECM that are observed in glaucoma.

Keywords: extracellular matrix, glaucoma anterior segment, matrix metalloproteinases, trabecular meshwork, endocytosis

Primary open angle glaucoma (POAG) is an irreversible blinding disease that is frequently associated with increased intraocular pressure (IOP).[1] Mutations in several genes have been found to cause POAG, but these mutations only account for 5% to 10% of all POAG cases.[2–5] At least 20 genetic loci have been identified indicating that POAG is a complex, genetically heterogeneous disease.[6] More recent studies have been performed to identify genetic risk factors for development of the disease, which has led to the identification of single nucleotide polymorphisms (SNPs) in several other genes.[7–9] One of these studies identified an SNP, rs4236601, located between caveolin-1 (CAV1) and caveolin-2 (CAV2) on chromosome 7q31.[10] This SNP was significantly associated with elevated IOP. Follow-up studies both confirmed and did not find association of this SNP with POAG.[11–14] Due to its association with elevated IOP, this suggests that CAV1 and/or CAV2 may play a critical functional role in the tissue responsible for establishing IOP, the TM, in the anterior segment of the eye.

Caveolins are the principal structural components of caveolae, which are 60- to 80-nm diameter invaginations in the plasma membrane that are essential for endocytosis, intracellular signaling, and cholesterol homeostasis.[15,16] There are three caveolin genes, CAV1, CAV2, and CAV3, with somewhat different expression patterns and functions. Caveolin-1 and CAV2 are abundant in nonmuscle cells, while CAV3 appears to be restricted to muscle cells.[16] Caveolin-1 monomers can homodimerize, but CAV1 can also heterodimerize with CAV2 via its C-terminus, and this interaction is required for localization of CAV2 to the plasma membrane.[17,18] More recent evidence shows that CAV2 can form homooligomeric complexes at the cell surface.[19] Genetic ablation of CAV1 in mice revealed its importance in caveolae formation.[20–22] Moreover, application of exogenous CAV1 led to de novo formation of caveolae, suggesting that CAV1 is an indispensable protein for both the structure and function of caveolae.[20,23] Conversely, knockout of CAV2 in mice had no apparent effect on caveolae formation in vivo leading to the assumption that CAV2 is not required to drive formation of caveolae.[24] In fact, CAV2 was retained in the Golgi and targeted toward the proteasomal degradation pathway in CAV1-deficient tissues.[20,25,26] This data led to the suggestion that some of the phenotypic changes in CAV1-null mice may be due to a concomitant reduction of CAV2.[24] More recent studies suggest

that CAV2 has discrete and separate biological functions than CAV1.[27]

Extracellular matrix (ECM) remodeling involves the synthesis, deposition, and degradation of matrix molecules.[28] Precise coordination of these complex events in normal tissues is critical to establish an ECM with correct organization and architecture. Disruption or dysregulation of ECM remodeling is associated with a variety of diseases, including many cancers and fibrotic diseases such as liver cirrhosis, pulmonary fibrosis, cardiovascular disease, and systemic sclerosis.[29] Following focal proteolytic degradation of ECM, partially degraded fragments are endocytosed by the cells and are either degraded intracellularly or are recycled back into the ECM. Cellular internalization of ECM fragments can provide a way to regulate the bioavailability of ECM fragments that may have potent effects. A role for CAVs in the endocytosis and recycling of ECM components is emerging.[30,31] For instance, CAV1 colocalizes with fibronectin in lipid rafts and knockdown of CAV1 results in stabilization of fibronectin matrix fibrils and a large decrease in fibronectin internalization and degradation.[32,33] Changes in ECM components were also observed in ECMs of fibroblasts derived from CAV1-null mice.[31] For instance, fibronectin fibrils assembled by wild-type fibroblasts were oriented more uniformly parallel than those assembled in CAV1-null fibroblasts, while collagen fibers were kinked and displayed a disturbed organization in knockout cells compared with wild-type. These alterations in ECM architecture and microenvironment led to changes in stiffness of the matrix. Atomic force microscopy revealed that wild-type ECMs were 40% stiffer than knockout ECMs.[31] Caveolins may also mediate focal proteolysis by matrix metalloproteinases (MMPs), since CAV1 colocalized with MMP-2 in caveolae, while CAV1$^{-/-}$ mouse hearts have increased MMP-2 activity.[34,35] Moreover, the scaffolding domain of CAV1 inhibited MMP2 activity in vitro.[34,36] Collectively, these studies describe a critical role for CAVs in defining ECM microenvironment, remodeling and maintaining normal tissue architecture.

In 2008, we described cellular structures in TM cells that are similar to podosomes and invadopodia of other cell types and we termed them PILS (podosome- or invadopodia-like structures).[37] These structures appeared to be sites of focal degradation and targeted turnover of ECM since MMP-2 and MMP-14 colocalized at these structures with cortactin, an archetypal protein of PILS.[37–39] These plaque-like structures are also strongly adhesive and provide a means by which the cell connects to the underlying ECM substrate.[38,40] Moreover, certain ECM molecules were localized at PILS, including versican, fibronectin, and integrins αV and β1. Thus, PILS are a center for sensing elevated IOP as well as mediating secretion and activation of proteolytic enzymes to focally degrade ECM in order to homeostatically adjust outflow resistance.[41]

Caveolins have previously been immunolocalized in TM cells.[42] The distribution of caveolins in the previous study strongly suggested to us that CAVs were localized at PILS. Thus, we hypothesized that CAVs may play a role in focal ECM degradation and endocytosis in TM cells, which could significantly affect outflow of aqueous humor through the TM. In this study, we evaluated the colocalization of CAV1 and CAV2 with cortactin at PILS in TM cells and tissue and generated CAV-silencing lentivirus to test the effect of CAV1 and CAV2 knockdown on outflow rates in anterior segment perfusion culture. The effects of CAV knockdown on MMP and ADAMTS4 enzyme levels and activity, fibronectin protein levels and TM cell cytoskeletal changes were also investigated.

Methods

Immunofluorescence and Confocal Microscopy

Primary TM cells were isolated from TM tissues dissected from porcine or human eyes as described previously.[43,44] Trabecular meshwork cells were grown on collagen-I–coated membranes (Flexcell; Flexcell International Corp., Hillsborough, NC, USA) since this provides a reduced stiffness substrate as compared to glass or plastic substrates, which is more similar to in situ conditions. Cell culture medium was medium glucose Dulbecco's modified Eagle's medium (DMEM) containing 1% penicillin-streptomycin-fungizone and with or without the addition of 10% fetal bovine serum. Cells were grown to approximately 80% confluence and then fixed with 4% paraformaldehyde, extracted with 0.05% Tween, and blocked with CAS-Block universal blocking agent (Cat #00-8120; Invitrogen, Grand Island, NY, USA) prior to immunostaining. Primary antibodies were: goat anti-CAV1 (AF5736; R&D Systems, Inc., Minneapolis, MN, USA), mouse anti-CAV1 (05-762), rabbit anti-MMP2 (Ab808), and mouse anti-MMP2 (MAb3308; all from EMD Millipore Corp., Billerica, MA, USA); rabbit anti-CAV1, rabbit anti-CAV2 and rabbit anti-MMP14 (Abcam Plc, Cambridge MA, USA); mouse anti-fibronectin and mouse anti-CAV2 (BD Transduction Laboratories, San Jose, CA, USA); rabbit anti-ADAMTS4 (MBL International Corp., Woburn, MA, USA); versican neo-epitope (PAI-1748A; Thermo Fisher Scientific, Inc., Rockford, IL, USA); total versican (Developmental Studies Hybridoma Bank, University of Iowa, Iowa City, IA, USA); total Erk1 (SC-93; Santa Cruz Biotechnology, Inc., Dallas, TX, USA); AlexaFluor 594 phalloidin (Molecular Probes, Eugene, OR, USA); and α-smooth muscle actin (αSMA; A2547; Sigma-Aldrich Corp., St. Louis, MO, USA). Secondary antibodies were AlexaFluor 594–conjugated anti-goat, AlexaFluor 488–conjugated anti-mouse, and AlexaFluor 594–conjugated anti-rabbit (Molecular Probes). Fluorescent stain 4′,6-diamidino-2-phenylindole (DAPI) was included in the mounting medium (ProLong; Invitrogen). Images were acquired with a laser scanning confocal microscope (Olympus Fluoview FV1000; Olympus Corp., Center Valley, PA, USA) with attached software (FV10-ASW; Olympus Corp.) and, where applicable, maintaining the same acquisition settings between control and CAV knockdown cells. Image processing software Fiji Is Just ImageJ (FIJI; provided in the public domain by http://fiji.sc/Fiji) was used to analyze images post acquisition.

For the frontal sections, a human anterior segment was immersion-fixed in 4% paraformaldehyde and frontal sections were cut.[45,46] Tissues were blocked and incubated overnight at 4°C with rabbit anti-CAV1 and mouse anti-CAV2 and primary antibodies were detected with AlexaFluor 488–conjugated anti-mouse and AlexaFluor 594–conjugated anti-rabbit secondary antibodies. Tissues were placed upright in mounting medium on glass slides and imaged by an inverted confocal microscope as above.

To quantitate the degree of colocalization in confocal images, we used image analysis software (Imaris Coloc; Bitplane USA, South Windsor, CT, USA) to calculate Pearson's correlation coefficients. This software estimates the degree of overlap between fluorescence signals obtained in two separate fluorescent channels.[47] Similarities in shape are considered, but differences in intensity are ignored. Raw compressed *z*-stacks acquired using sequential scanning on the confocal were analyzed. Background correction values were identical for each image and a whole field of view was used as the input. The Pearson's coefficients were calculated from multiple images ($n = 2$–7) and then averaged and a standard error of the mean was calculated. The degree of colocalization from the Pearson's values was categorized as very strong (0.85–1.0);

strong (0.49–0.84); moderate (0.1–0.48); weak (–0.26 to 0.09); and very weak (–1 to –0.27) as described previously.[48]

Generation and Characterization of CAV Gene shRNA Silencing Lentivirus

Short, hairpin RNA (shRNA) vectors were generated in order to silence CAV1 and CAV2 as previously described.[5,45,49] Briefly, the online designer (BLOCK-iT RNAi; Invitrogen) was used to design shRNA targeting CAV1 (#1 matches pig; #6 matches human) and CAV2 (#13 targets both human and pig sequences). The sequences of the silencing primers were

1. CAV1 #1: 5′-CACCGAACTCAAACTGAGGAATTTCCGAA GAAATTCCTCAGTTTGAGTTC-3′;
2. CAV1 #6: 5′-CACCGCTTTGGACCTAATCCAAGCAC GAATGCTTGGATTAGGTCCAAAGC-3′; and
3. CAV2 #13: 5′-CACCGCCTTCAGTGCAGACAATATGC GAACATATTGTCTGCACTGAAGGC-3′.

A shRNA control (shCtrl) that does not target any other known human or porcine gene has been previously characterized.[45,49] Double-stranded shRNAs were cloned into the pENTR/U6 vector using T4 ligase (Invitrogen) and the sequences were verified by DNA sequencing. The shRNA cassette was transferred into the pLenti6/BLOCK-iT-DEST vector (HIV-based lentiviral vector) by LR Clonase (Invitrogen) recombination. Replication incompetent lentivirus was generated by cotransfecting 3 μg pLenti silencing plasmid and 9 μg packaging mix (ViraPower; Invitrogen) into 293FT cells using a commercial reagent (Lipofectamine 2000; Invitrogen). Lentiviral-containing supernatants were harvested 72 hours post transfection and viral titers were calculated in plaque formation units.[45,49]

Western Immunoblotting

Porcine or human TM cells were infected with control or CAV-silencing lentivirus for 72 hours. Serum-free media was then added for an additional 48 hours. Radioimmunoprecipitation assay (RIPA) cell lysates and serum-free media were harvested. Proteins were separated on 10% SDS-PAGE gels (Bio-Rad Laboratories, Inc., Hercules, CA, USA) under reducing conditions and transferred to nitrocellulose. Primary antibodies were selected from those described above. Secondary antibodies were infrared dye–conjugated anti-rabbit and infrared dye–conjugated anti-mouse (IRDye 700 and IRDye 800; Rockland Immunochemicals, Inc., Gilbertsville, PA, USA). Western immunoblots were imaged using an infrared imaging system (Odyssey CLx; LI-COR Biosciences, Inc., Lincoln, NE, USA). Bands were quantitated using ImageJ software (http://imagej.nih.gov/ij/; provided in the public domain by the National Institutes of Health (NIH), Bethesda, MD, USA); following background correction and values were then normalized to extracellular signal-regulated kinase 1 (ERK1) as a loading control.[50] Mean pixel intensity was determined from three independent experiments and a standard error of the mean was calculated.

Anterior Segment Perfusion Culture

Short hairpin–CAV silencing lentivirus was applied to human or porcine anterior segments in perfusion culture as described previously.[5,45,49] Human donor eye pairs were acquired from Lions Eye Bank of Oregon (Portland, OR, USA) within 24 to 48 hours of death. The average age of donor eyes was 84.75 ± 7.7 years, age range 68 to 90 years. Human anterior segments were placed into serum-free stationary organ culture 5 to 7 days prior to perfusion culture to allow for cellular recovery. Human donor tissue protocols were approved by the Oregon Health & Science University Institutional Review Board and were conducted in accordance to the tenets of the Declaration of Helsinki. Porcine eyes were acquired from the local slaughterhouse within 4 hours of death and immediately placed into perfusion culture.

Anterior segments were set up in perfusion culture using a constant pressure system as described previously.[45,51,52] Following stabilization of flow rate, shCAV or shCtrl lentivirus (10^8 pfu) was applied as a bolus to the perfusion chambers by media exchange (indicated by time point 0) and outflow facility was measured for an additional 3 to 5 days. Change in outflow facility was determined by dividing flow rates after treatment by the average outflow rate prior to treatment. Data from individual eyes were then combined and averaged. Significance was determined by one-way ANOVA. At the end of the experiment, anterior segments were removed from the perfusion chambers and tissues were fixed in 4% paraformaldehyde. Serial radial sections measuring 5 μm were cut approximately perpendicular to Schlemm's canal (SC) at the histopathology core facility of the Knight Cancer Institute (Oregon Health & Science University, Portland, OR).[51] Sections were deparaffinized, blocked, and incubated with rabbit anti-fibronectin primary antibody. Secondary antibodies were AlexaFluor 594–conjugated anti-rabbit antibodies. Tissue sections were visualized with a laser confocal scanning microscope (Olympus Corp.) with associated software, and images were processed with Fiji image processing software. Some sections were stained with hematoxylin and eosin (H&E).

Proteolytic Degradation of Gelatin by TM Cells

To assess proteolytic degradation, culture dishes (Delta T; Bioptechs, Inc., Butler, PA, USA) were coated with conjugated gelatin (20 μg/mL, Oregon Green 488; Life Technologies, Grand Island, NY, USA) for 2 hours with gentle rocking at room temperature. The gelatin mix was rinsed off with 1× Dulbecco's PBS and the conjugated gelatin was cross-linked for 7 minutes with 0.5% glutaraldehyde. Dishes were washed extensively with PBS prior to the addition of 1.0 M Tris-HCl (pH: 6.8) overnight at 4°C to terminate the cross-linking reaction. After further washing, TM cells were plated on the coated dishes for 2 hours in 0.1% serum-containing DMEM prior to confocal microscopy. Fiji image processing software was used to quantify gelatin degradation by TM cells using a previously described method.[53] An identical scale and measurement was set up for all images. Images were thresholded to set the upper and lower pixel intensities and the same threshold was applied to all images. Since the coverslips are not uniformly flat, there may be some unevenness of the gelatin coating. To overcome these potential variations, background was eliminated by filtering with a bandpass filter. A particle size > 0 was used to remove noise from the selected area in the "analyze particles" function. The functions "show outlines" and "include holes" were used to identify areas of matrix degradation in each image. Data from individual images were averaged, a standard error of the mean was calculated, and the data were subjected to ANOVA statistical analysis.

MMP and ADAMTS4 Activity Assays

A generic MMP assay kit (SensoLyte 520 Generic MMP Assay Kit; AnaSpec, Inc., Fremont, CA, USA) was used to measure MMP activity and an ADAMTS/aggrecanase assay kit (SensoLyte 520 Aggrecanase-1 Assay Kit; AnaSpec, Inc.) was used to detect ADAMTS4 activity. Both of these assays use the same principle: a quenched fluorescence resonance energy transfer peptide is

Investigative Ophthalmology & Visual Science

used as a substrate, which, upon cleavage by the enzyme, generates fluorescence that can be quantitated in a plate reader. Relative fluorescent units (RFUs) are directly correlated to enzyme activity. For the MMP assay, we chose to use a generic substrate that can be cut by MMPs 1 through 3, 7 through 9, and 12 through 14. A different peptide substrate was used for the ADAMTS4 assay. Cleavage of this peptide by other aggrecanases and MMPs is negligible.

Control and CAV1- or CAV2-silenced TM cells were changed into serum-free media for 48 hours and conditioned media and cell lysates were harvested using buffer supplied with the kit and addition of protease inhibitor cocktail. Following centrifugation (×1000*g* for 15 minutes at 4°C), MMPs in each sample were activated with 1 mM 4-aminophenylmercuric acetate for 90 minutes at 37°C. No such activation step is required for ADAMTS4. The quenched peptide substrate was then incubated with the samples in a 96-well format for 60 minutes at room temperature. Relative fluorescence units were read at excitation/emission wavelengths (490/520 nm). Total protein in each sample was measured using a bicinchoninic acid assay kit (Pierce Biotechnology, Inc., Rockford, IL, USA). The results are presented as RFUs/total protein. Data from five independent experiments was averaged and a standard error of the mean was calculated. Significance was determined by one-way ANOVA.

Fibronectin ELISA assay

A fibronectin ELISA assay was performed to quantitate the concentration of fibronectin in control and CAV-silenced TM cells. Lentivirus-infected TM cells were plated in triplicate in 24-well plates. After 72 hours, cell lysates were harvested in RIPA buffer containing 2 M urea, to aid solubilization of fibronectin fibrils, and protease inhibitor cocktail (Sigma-Aldrich Corp.). Fibronectin concentration in each sample was quantitated using a competitive inhibition ELISA kit (QuantiMatrix Human Fibronectin ECM300; EMD Millipore Corp.) following the manufacturer's instructions. A standard curve was included on the plate. Each sample was read in triplicate and fibronectin concentration determined from interpolation onto the curve. Values from the individual samples were then averaged and then data from three independent experiments were averaged and a standard error of the mean was calculated. Analysis of variance was used to determine significance. A P value < 0.05 was considered significant.

Results

CAVs Are Localized at PILS, Areas of Focal ECM Degradation

In other cell types, CAV1 is located at the plasma membrane, whereas CAV2 is localized to the Golgi and is only redistributed to the plasma membrane when CAV1 is coexpressed.[25] Therefore, we investigated the cellular distribution of endogenous CAV1 and CAV2 in human TM cells and tissue (Fig. 1). We found partial colocalization of CAV1 and CAV2 in TM cells. CAV1 (green) was found in discrete regions of cellular staining at what appeared to be PILS. In addition to regions of colocalization with CAV1, CAV2 (red) also showed areas of punctate dots throughout the cytoplasm (Figs. 1A, 1D). Since the pattern of CAV staining was similar to the distribution of PILS, each CAV was colocalized with cortactin, an archetypal biomarker of PILS.[38] Both CAV1 (red; Figs. 1B, 1E) and CAV2 (red; Figs. 1C, 1F) showed substantial colocalization with cortactin (green). Image analysis software (Bitplane USA) was used to generate a Pearson's correlation coefficient to quantitate the degree of colocalization of CAVs with cortactin (Table). Pearson's values of 0.515 ± 0.041 for CAV1 and 0.530 ± 0.107 for CAV2 indicates "strong" colocalization of CAVs with cortactin based on a previously described classification of colocalization.[48]

The colocalization of CAV1 (green) and CAV2 (red) in a frontal section of human TM tissue is also shown (Figs. 1G, 1H). Both CAVs were detected in the outer TM beams, in the juxtacanalicular (JCT) region adjacent to Schlemm's canal and at the inner wall (IW) endothelium. Caveolin-2 staining (red) had higher signal in the JCT and inner wall endothelium area than in the outer TM beams, whereas CAV1 (green) was distributed throughout the TM. Areas of CAV colocalization (orange/yellow) were primarily detected in the JCT region.

Effects of CAV Gene Knockdown on TM Outflow Rates

The SNP between the CAVs that was identified in glaucoma patients with elevated IOP suggests a role for CAVs in aqueous humor outflow regulation.[10,11] To evaluate the effects of CAV knockdown on outflow, we generated CAV silencing lentivirus and applied them to anterior segment perfusion cultures. Short hairpin RNA constructs were developed targeting the CAV1 and CAV2 genes. Two CAV1 constructs were generated, since a target sequence could not be identified that was common to both species. Short hairpin CAV1 #1 targeted porcine CAV1, while shCAV1 #6 targeted human CAV1. The CAV2 construct (shCAV2 #13) targeted an identical sequence in the human and porcine gene. A control silencing lentivirus was generated and described previously.[45] Efficacy of each construct in reducing their respective CAV protein was assessed by Western blotting (Figs. 2A, 2B). Densitometry of Western bands showed that CAV1 was reduced by approximately 65% and CAV2 protein was reduced by approximately 95% compared with shControl-infected cells.

Short hairpin CAV silencing lentivirus was then applied as a bolus to porcine and human anterior segments in perfusion cultures. Outflow facility was measured for a further 70 hours (porcine; Fig. 2C) or 122 hours (human; Fig. 2D). Silencing of CAV1 increased outflow facility, while silencing of CAV2 decreased outflow facility in both species. Human anterior segments displayed a greater response (4- and 0.3-fold for shCAV1 and shCAV2, respectively) than porcine anterior segments (1.5- and 0.7-fold for shCAV1 and shCAV2, respectively). Moreover, human anterior segments tended to respond faster than porcine eyes with significant effects observed at 28 hours in humans compared with 50 hours in porcine eyes. Outflow facility effects were similar when using a second shRNA construct for each CAV gene (not shown), supporting the specificity of the effects.

Effects of CAV Gene Knockdown on ECM Degradation by MMPs

Application of MMPs to anterior segments in perfusion culture increases outflow.[54] We therefore hypothesized that CAVs may modulate outflow resistance via altering MMP levels, cellular localization, and/or activity. Thus, we evaluated localization of endogenous CAV1 and CAV2 with MMP2 and MMP14 in primary cultured TM cells (Fig. 3). Caveolin-1 (red) showed partial colocalization with MMP2 (green; Fig. 3A), while CAV2 showed stronger colocalization with MMP2 (Fig. 3B). Matrix metalloproteinase-14 (green) showed partial colocalization with CAV1 (red; Fig. 3C) and CAV2 (red; Fig. 3D). However, both MMP2 and MMP14 also showed abundant immunostaining that was not associated with either of the CAVs. Pearson's values were calculated and showed that MMP14 and CAV2 had "very strong" colocalization, MMP2 and CAV2 and MMP14 and

Investigative Ophthalmology & Visual Science

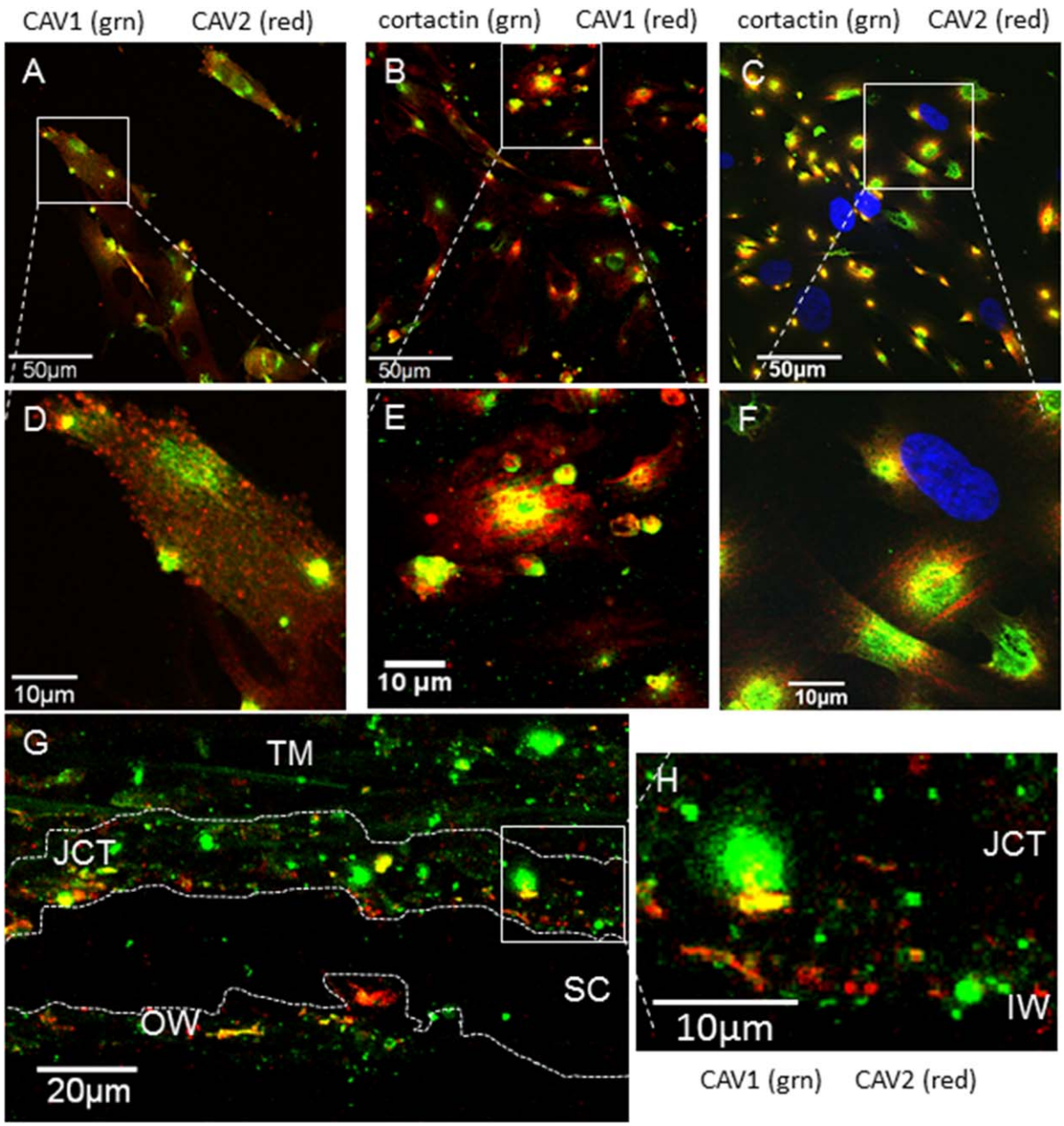

Figure 1. Colocalization of caveolins-1 and -2 with each other and with cortactin, a biomarker of PILS. (**A**) Localization of CAV1 (*green*) and CAV2 (*red*) in human TM cells. (**B**) Caveolin-1 (*red*) localized with cortactin (*green*). (**C**) Caveolin-2 (*red*) localized with cortactin (*green*). We used DAPI to stain nuclei *blue*. (**D–F**) Show higher magnification images of the *boxed areas* in (**A–C**). (**G**) A frontal section of human TM tissue immunostained with CAV1 (*green*) and CAV2 (*red*). Partial colocalization was observed, particularly in the JCT region adjacent to Schlemm's canal. The TM beams show slight green autofluorescence. A *dotted line* delineates the wall of SC and another *dotted line* shows approximately the depth of the JCT region (7–20 μm from the IW). (**H**) Shows a higher magnification image of the *boxed area* in (**G**). *Scale bars*: (**A–C**) 50 μm; (**G**) 20 μm; (**D–F**, **H**) 10 μm.

CAV1 were categorized as "strong," and MMP2 and CAV1 showed "moderate" colocalization (Table).

Next, we investigated ECM degradation in CAV-silenced human TM cells. Trabecular meshwork cells were infected with shControl or shCAV silencing lentivirus and plated on gelatin-488 coated dishes to monitor ECM degradation. Two hours after plating, control TM cells showed diffuse patches where the gelatin-488 had been degraded (arrows; Fig. 3E). In shCAV1 (Fig. 3F) and shCAV2 (Fig. 3G) knockdown cells, areas of degradation were more distinctive, suggesting increased focal degradation of gelatin compared with control cells. The amount of degradation was analyzed with Fiji image processing software using a previously described method.[53] A significant increase in the amount of gelatin degradation was observed in CAV-silenced TM cells (Fig. 3H).

To assess whether this increased degradation was due to differences in MMP activity, we measured MMP activity using a quenched fluorogenic peptide that releases fluorescence upon proteolytic cleavage by a MMP. We chose a generic MMP peptide that can be cleaved by multiple MMPs including MMPs 1 through 3, 7 through 9, and 12 through 14. Fluorescence generated is directly related to enzyme activity. In the media, there was a significant increase in MMP activity in both shCAV1- and shCAV2-silenced cells compared with control-

Investigative Ophthalmology & Visual Science

Table. Pearson's Correlation Coefficients Between Endogenous CAV1 or CAV2 and MMP2, MMP14, or Cortactin

Protein 1	Protein 2	Pearson's Correlation Coefficient	Degree of Colocalization
CAV1	MMP2	0.327 ± 0.056	Moderate
	MMP14	0.555 ± 0.097	Strong
	Cortactin	0.515 ± 0.041	Strong
CAV2	MMP2	0.540 ± 0.029	Strong
	MMP14	0.897 ± 0.1009	Very strong
	Cortactin	0.530 ± 0.107	Strong

Calculated using image analysis software (Bitplane USA). Mean Pearson's coefficient ± SEM of compressed confocal *z*-stacks ($n = 2$–7). Degrees of colocalization were based on a previously published classification system.[48]

infected cells (Fig. 3I). Matrix metalloproteinase activity in cell lysates was also increased upon CAV silencing, but these changes were not significantly different.

Western immunoblots were then performed on serum-free media and cell lysates from shCtrl and shCAV-infected cells (Fig. 3J). The levels of MMP14, a transmembrane MMP that activates the proform of MMP2, were assessed in cell lysates. The only difference observed was a reduction in the proform of MMP14 (66 kDa; arrow) in shCAV1-infected TM cells. Protein levels of MMP2 in media were also assessed. When equal amounts of total protein were loaded into each well, an increase in MMP2 was apparent in the media of both shCAV1- and shCAV2-infected cells compared with control-infected cells (Fig. 3J, lowest panel). Densitometry of this MMP2 band revealed an average increase of 1.69 ± 0.203 for shCAV1 (mean ± SEM; $n = 4$) and a 1.74 ± 0.43–fold increase for shCAV2 compared with control-infected cells.

Effects of CAV Silencing on ADAMTS4

Another MMP that appears to be involved in altering outflow resistance is ADAMTS4.[52] This enzyme cleaves the proteoglycan, versican, to expose a neoepitope in the large chondroitin sulfate-substituted domain. An antibody has been developed to specifically recognize this versican neoepitope, which can be used as an indicator of ADAMTS4 activity. Therefore, we investigated the colocalization of endogenous CAVs with versican neoepitope in TM cells. There was some colocalization of the versican neoepitope antibody (green) with CAV1 (Fig. 4A; red) and CAV2 (Fig. 4B; red). Not surprisingly, ADAMTS4 (red) also showed strong colocalization with CAV1 (Figs. 4C, 4D; green) and CAV2 (Figs. 4E, 4F; green). Immunostaining of ADAMTS4 was in very discrete punctate dots, which were clustered at PILS, but also appeared as individual vesicles throughout the cell. Immunostaining of ADAMTS4 was also assessed in CAV-silenced TM cells. In CAV1-silenced cells (Fig. 4H), there appeared to be more clustering of ADAMTS4-stained vesicles compared with control cells. In CAV2-silenced cells, ADAMTS4 showed a large increase in the number of single intracellular punctate vesicles (Fig. 4I) compared with shControl-infected cells (Fig. 4G). This apparent increase in the number of ADAMTS4-stained vesicles suggested that ADAMTS4 enzyme activity may be altered in CAV-silenced cells. Therefore, we

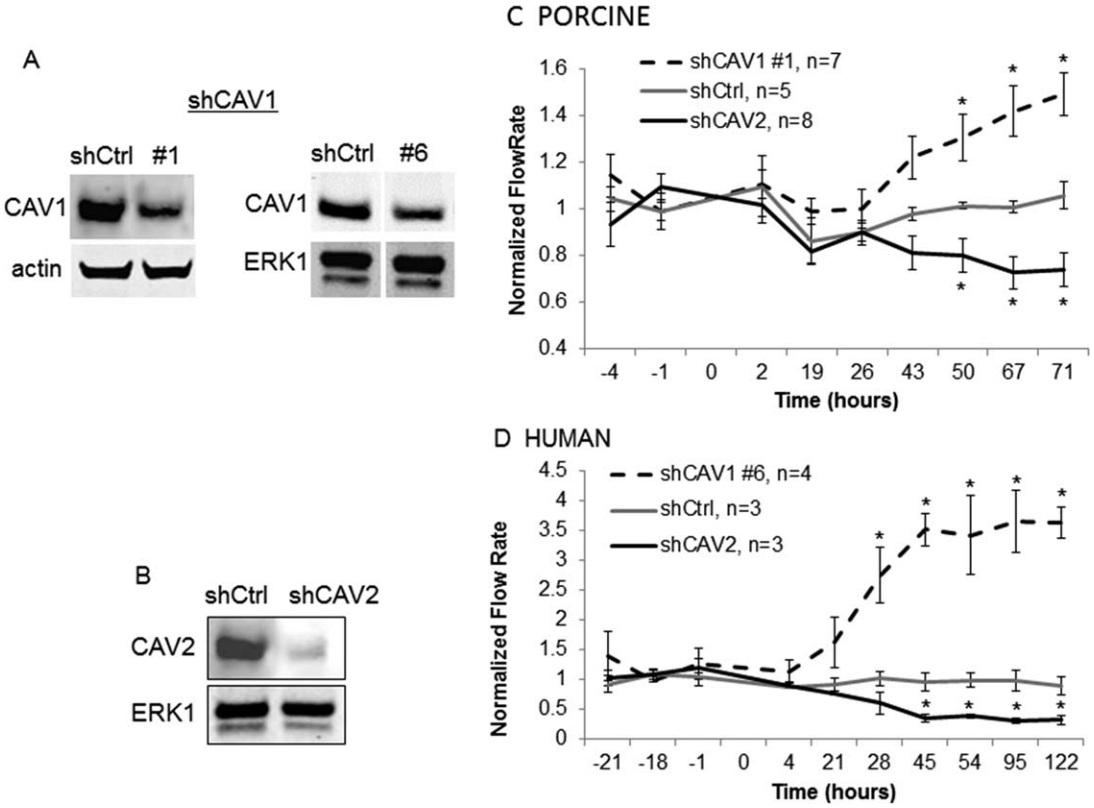

Figure 2. Caveolin shRNA gene silencing. (**A**) Western immunoblotting shows a significant decrease in CAV1 protein in shCAV1-infected compared with control (shCtrl) in TM cells. Actin or total ERK1 loading controls are shown. (**B**) Western immunoblotting shows a significant decrease in CAV2 protein in control (shCtrl) and shCAV2-infected TM cells. Total ERK1 loading control is shown. In perfused porcine (**C**) and human (**D**) anterior segments, shCAV1 significantly increased outflow rates over time, while shCAV2 decreased outflow rates. Time 0 indicates the time of application of lentivirus. Data show the average flow rate ± SEM; *n* is indicated in the graph legend. *$P < 0.05$ by ANOVA.

Investigative Ophthalmology & Visual Science

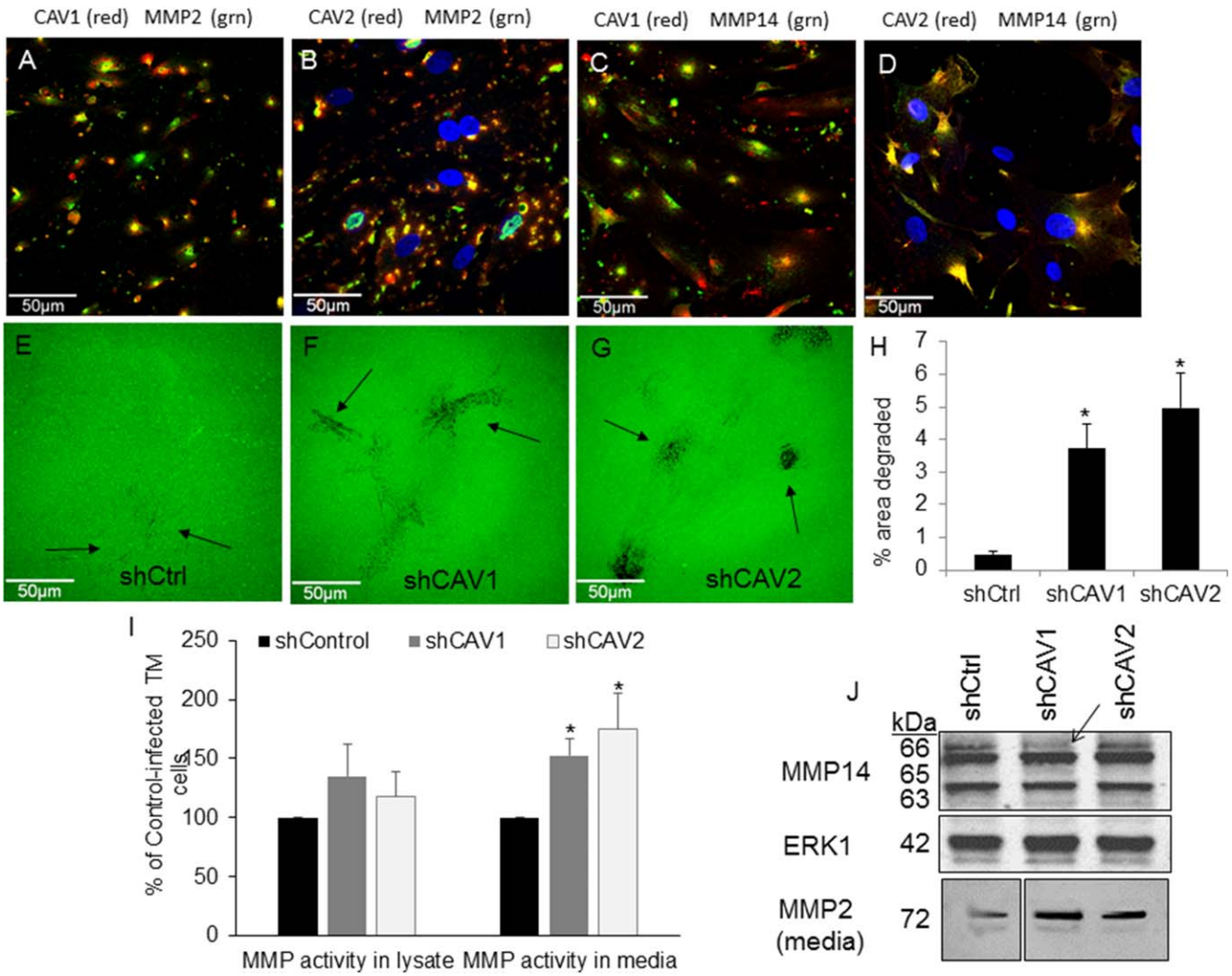

Figure 3. Effects of CAV silencing on MMP levels and activity. Localization of endogenous CAV1 ([**A**, **C**], *red*) or CAV2 ([**B**, **D**]; *red*) compared with MMP2 ([**A**, **B**]; *green*) or MMP14 ([**C**, **D**]; *green*) are shown in human TM cells. We used DAPI to stain nuclei *blue*. (**E**–**G**) Degradation of Oregon Green 488–conjugated gelatin (Life Technologies) 2 hours after plating control (**E**), CAV1- (**F**), and CAV2-silenced (**G**) human TM cells. *Arrows* point to areas of degradation. *Scale bars*: 50 μm. (**H**) Quantitative analysis of the areas of gelatin degradation using Fiji image processing software. Data is averaged (±SEM) from multiple images: $n = 5$ for shControl; $n = 9$ for shCAV1; $n = 6$ for shCAV2. $^*P < 0.01$. (**I**) Activity of MMP was measured in cell lysates and media using a fluorogenic MMP assay with a generic peptide substrate. Results show RFUs normalized to total protein in each sample and calculated as a percentage of control. *Error bars* represent SEM. $^*P < 0.05$ by ANOVA; $n = 5$. (**J**) Western immunoblots of MMP14 in cell lysates and MMP2 in media of control- and CAV-infected TM cells. *Arrow* points to a reduction of the proform of MMP14 in sh*CAV1*-silenced TM cells. Total ERK1 was used as a loading control for lysates. For the media lanes, equal amounts of total protein were loaded. Positions of molecular weight markers are shown in kDa.

quantitated the amount of versican neoepitope generated in Western immunoblots and measured enzyme activity using a quenched fluorogenic peptide substrate specific for ADAMTS4. Trabecular meshwork cell lysates from CAV-silenced and control-infected lysates were separated by SDS-PAGE. Western immunoblots (Fig. 4J) showed that total versican protein levels were slightly increased 1.15-fold in CAV knockdown cells compared with controls. The versican neoepitope band (70 kDa) was also increased in CAV knockdown cells compared with control. When this band was normalized to the amount of total versican in each lane, there was a 123% and 121% increase for CAV1- and CAV2-silenced cells, respectively. Finally, using the fluorogenic peptide assay, ADAMTS4 enzyme activity in TM cell lysates was quantitated (Fig. 4K). There was a 1.71 ± 0.15–fold significant increase ADAMTS4 activity in CAV1-silenced TM cells and a 1.51 ± 0.22–fold increase in CAV2-silenced cells (mean ± SEM; $n = 5$). Unlike the MMP assay above, ADAMTS4 activity was only detected in cell lysates and was not detected in the medium (not shown).

Effects of CAV Silencing on Fibronectin

A previous study implicated CAV1 with the endocytosis and recycling of fibronectin.[33] However, no studies have investigated the contribution of CAV2 to fibronectin turnover. Therefore, we examined fibronectin assembly and concentration in CAV knockdown TM cells. First, we evaluated colocalization of endogenous CAV1 and CAV2 with fibronectin. There were few areas of colocalization of CAV1 or CAV2 (red) with fibronectin (green; Figs. 5A, 5B). This was not surprising as these are usually located in different cellular compartments. The distribution of fibronectin in CAV knockdown TM cells was also analyzed. An increase in fibrillar fibronectin immuno-

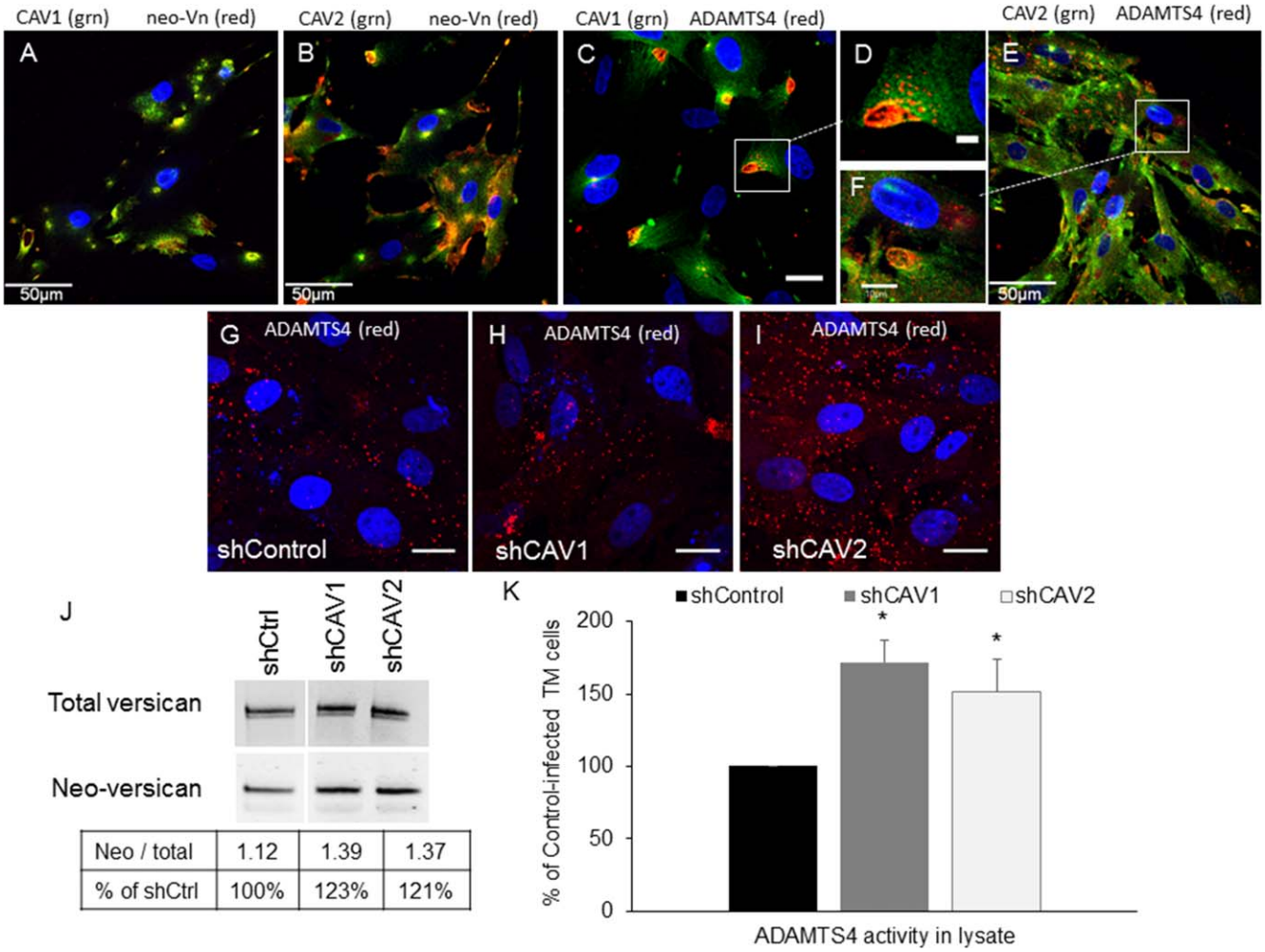

Figure 4. Effects of CAV silencing on ADAMTS4 immunolocalization and activity. Colocalization of endogenous CAV1 ([**A**, **C**, **D**]; *green*) and CAV2 ([**B**, **E**, **F**]; *green*) with versican neoepitope ([A, **B**]; *red*) and ADAMTS4 ([**C**–**F**]; *red*). Versican neoepitope (neo-Vn) is exposed following proteolytic cleavage by ADAMTS4. (**G**–**I**) Immunostaining with ADAMTS4 immunostaining of control (**G**), CAV1- (**H**) or CAV2-silenced (**I**) human TM cells. We used DAPI to stain nuclei *blue*. *Scale bars*: (**A**, **B**, **E**) 50 μm; (**C**, **G**–**I**) 20 μm; (**F**) 10 μm; (**D**) 5 μm. (**J**) Western immunoblots showing total versican and neo-Vn epitope bands in control and CAV-silenced TM cells. The Table shows the densitometry ratio of neoepitope to total versican for each condition and then calculated as a percentage of the control. (**K**) ADAMTS4 activity in cell lysates was quantified by a fluorogenic enzyme activity assay. Results show RFUs normalized to total protein in each sample. *Error bars* represent SEM. $^*P < 0.05$ by ANOVA; $n = 5$.

staining was apparent in CAV-silenced TM cells (Figs. 5D, 5E) by immunofluorescence and fibrils appeared thicker than in control-infected cells (Fig. 5C). Radial sections of human TM perfused with control and CAV-silencing lentivirus were also immunostained with fibronectin antibodies. A large increase in fibronectin immunostaining was observed in sections where CAVs had been silenced (Figs. 5G, 5H) compared with control anterior segments (Fig. 5F). The increased fibronectin immunostaining was most apparent at the inner wall of Schlemm's canal and in the underlying JCT region, within approximately 5 μm of the inner wall. There was also increased fibronectin immunostaining located at the outer wall (OW) of Schlemm's canal and, although less apparent, in the corneoscleral meshwork TM beams of CAV knockdown tissue. Increased fibronectin immunostaining in tissues correlates with the increased fibrillar fibronectin staining in CAV-silenced TM cells. Stained H&E sections of shControl and CAV-silenced TM from human and porcine eyes are shown in Supplementary Figure S1.

Western immunoblots and an ELISA assay were then used to quantitate fibronectin levels. By Western blot, there was a large increase in fibronectin in the media in knockdown cells (Fig. 5I). Densitometry showed an approximately 2-fold increase in fibronectin in the media of CAV knockdown cells. By ELISA assay, fibronectin concentration was significantly increased in CAV knockdown cells compared with shControl cells (Fig. 5J). When the results were calculated as a percentage, CAV1 knockdown caused a 43% and 27% increase compared with control cells for #1 and #6, respectively, while CAV2 knockdown caused a 39% increase in fibronectin concentration.

Effects of CAV Silencing on TM Cell Cytoskeleton Components

Caveolins have also been implicated in regulating cellular contractility via the actin-based cytoskeleton and cell contractility has been linked to expression of α-smooth muscle actin (αSMA).[31,55] Therefore, we assessed the distribution of actin and αSMA in CAV knockdown TM cells. Phalloidin-594 was used to stain F-actin and there was a distinctive increase in stress fibers in CAV knockdown cells (Figs. 6B, 6C) compared with control cells (Fig. 6A). Levels of αSMA appeared to be

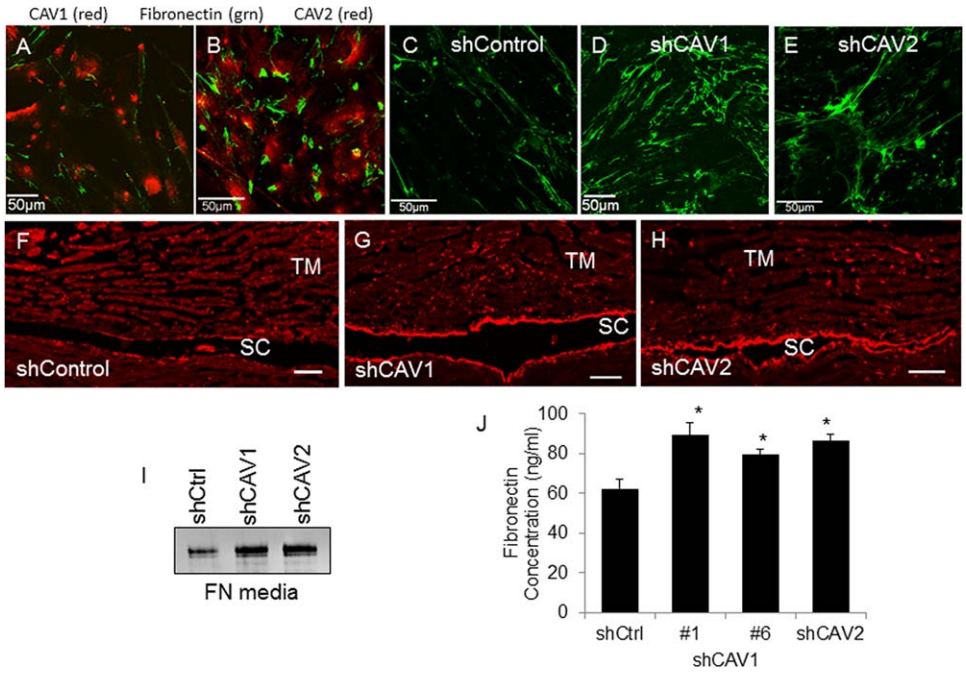

Figure 5. Effects of CAV silencing on fibronectin. Colocalization of endogenous CAV1 ([**A**]; *red*) and CAV2 ([**B**]; *red*) with fibronectin (*green*). Fibronectin immunostaining in control (**C**, **F**), CAV1- (**D**, **G**) and CAV2-silenced (**E**, **H**) TM cells (**C**–**E**) and radial sections of perfused human anterior segments (**F**–**H**). Confocal acquisition settings were identical for control and CAV-silenced cells. *Scale bars*: (**A**–**E**) 50 μm; (**F**–**H**) 20 μm. (**I**) Western immunoblot analysis of fibronectin levels in the media of control and CAV-silenced TM cells. Equal amounts of protein were loaded into each lane. (**J**) A fibronectin ELISA assay of control and CAV-silenced human TM cell lysates. Data is the mean ± SEM; $n = 3$. $^*P < 0.05$ compared with shControl by ANOVA.

increased and labeling was more defined in CAV-knockdown TM cells (Figs. 6E, 6F) than in control cells (Fig. 6D). Merged panels of phalloidin and αSMA are also shown (Figs. 6G–I).

Discussion

Caveolins-1 and -2 have be implicated in the pathogenesis of glaucoma.[10,42] In the original paper, an SNP was identified between the *CAV1* and *CAV2* genes, but the authors could not conclude which gene was the culprit for causing glaucoma. From our perfusion culture data, we found a significant increase in outflow rate upon *CAV1* silencing, but a decrease in outflow rate upon *CAV2* silencing. Since decreased outflow rates are consistent with elevated pressure, our data suggests that CAV2 is the most likely candidate for causing increased IOP in glaucoma patients harboring the SNP. Another study showed that the amount of CAV1 protein detected in human TM tissue was similar between individuals, irrespective of whether they had glaucoma or not, but CAV2 protein levels were highly variable between individuals.[42] Collectively, this suggests that endogenous levels of CAV2 may be more important than CAV1 levels and this may partially govern the susceptibility of a patient to developing elevated IOP and glaucoma.

It remains unclear as to why knockdown of each *CAV* would cause opposite effects on outflow. There were differences in the efficacy of silencing each *CAV*, which may partially account for the observed differences; the *CAV2* silencing construct was much more efficient at protein knockdown than either of the *CAV1* constructs. However, each CAV has different functions in cell signaling. Although CAV2 is highly homologous to CAV1 protein, the G-protein binding region only shows approximately 30% homology. This region of CAV2 was shown to exhibit GTPase activating protein (GAP) activity, whereas the corresponding region of CAV1 suppresses GTPase activity and acts as a guanosine diphosphate (GDP) dissociation inhibitor (GDI).[17] In caveolae, there appears to be a two-step mechanism to recruit and sequester inactive G proteins in the membrane: CAV2 acts as a GAP to place activated G-proteins in the inactive GDP-bound conformation and the CAV1 functions as a GDI to keep them in an inactive conformation. Thus, in *CAV2*-silenced anterior segments, a reduction in GAP activity and recruitment of G proteins to the caveolae membrane could activate different downstream cell signaling events than *CAV1* silencing and lead to the observed opposite effects on outflow.

Alterations in ECM turnover may also contribute to the difference in outflow observed since ECM is thought to be a key source of resistance to aqueous outflow.[28,41] Knockdown of both *CAV*s significantly increased both MMP and ADAMTS4 activity. This is consistent with increased MMP2 activity in *CAV1*-null mouse hearts.[34,35] We observed a reduction in the proform of MMP14 in *CAV1*-silenced cells, but not *CAV2*-silenced cells, suggesting that MMP14 was in a more active state. This is a major difference since active MMP14 activates MMP2, which has a potent effect on outflow.[54] A slight shift in the enzymatic balance and/or activation of MMPs in response to *CAV* knockdown could profoundly influence the composition and structure of the ECM and this is likely to be different for each CAV. However, degradation is only one aspect in ECM turnover. Caveolins are also involved in uptake of proteolytic ECM fragments. Caveolin-1 and CAV2 may be involved in the differential uptake of these fragments, triggering activation of different cell signaling pathways to induce synthesis of different replacement ECM. Changes in the structure, amount, and deposition of replacement matrix caused by silencing of each *CAV* will profoundly influence the microenvironment of the ECM in the flow channels leading to increased or decreased outflow. Thus, differences in the degradation rates, target ECM

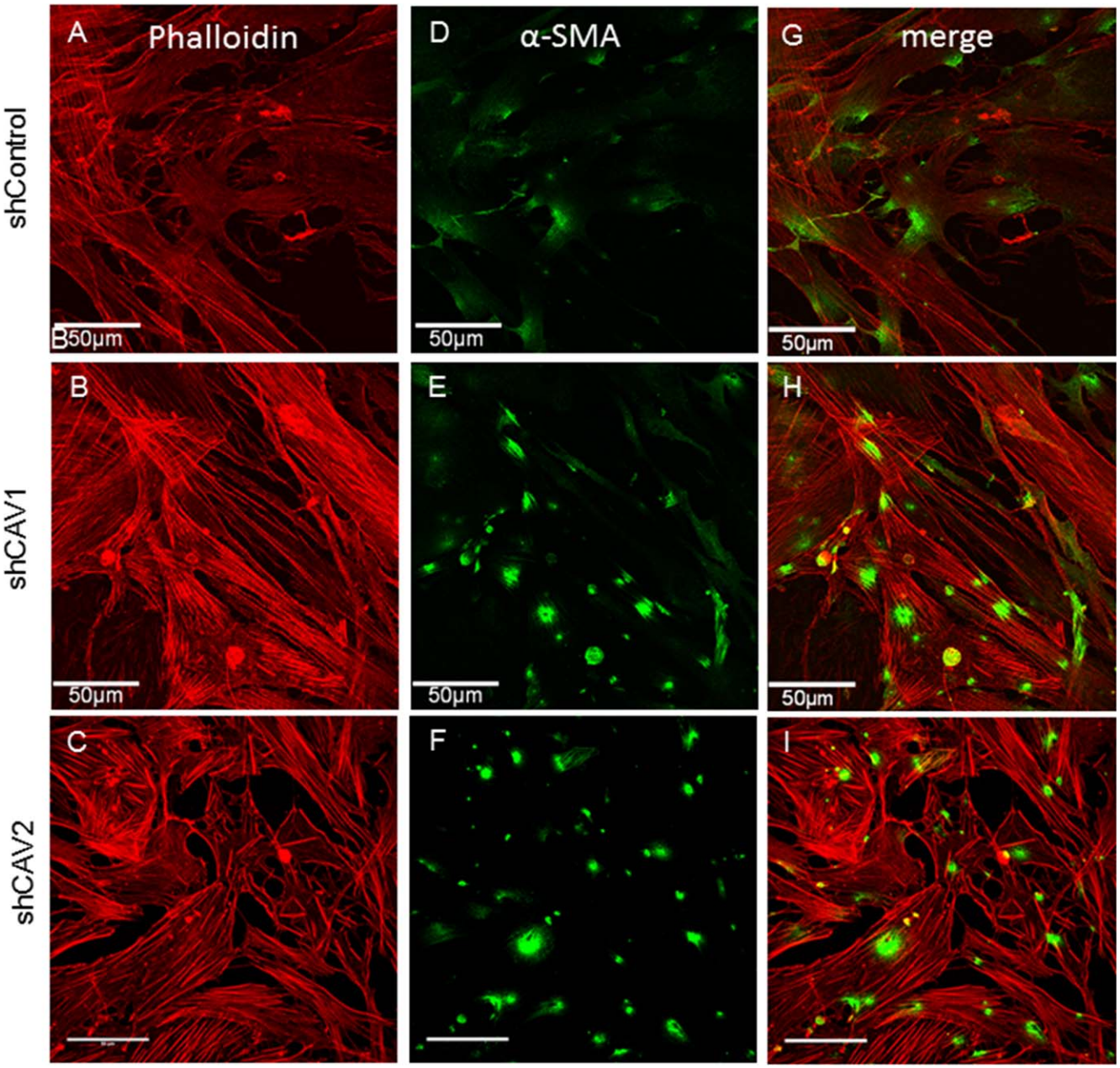

Figure 6. Effects of CAV silencing on the actin cytoskeleton. Human TM cells were infected with control (**A**, **D**, **G**), CAV1-silencing (**B**, **E**, **H**), or CAV2-silencing (**C**, **F**, **I**) lentivirus. F-actin was stained with phalloidin-594 (*red*; [**A–C**], [**G–I**]) and αSMA immunostaining of CAV-silenced TM cells (*green*; [**D–F**], [**G–I**]). The merged images are shown (**G–I**). Confocal acquisition settings were identical for control and CAV-silenced cells. *Scale bars*: 50 μm.

molecules, endocytosis of ECM fragments and/or deposition of replacement ECM could all contribute to the opposite effects on outflow that is observed in *CAV*-silenced anterior segments. Further studies will be required to clarify the nuances of ECM proteins that display differential levels, degradation and/or activities upon silencing of each *CAV*. Caveolae are also abundant in SC endothelial cells.[56,57] Although the majority of the resistance appears to reside in the JCT, SC inner wall endothelium contributes approximately 10% of the resistance.[58] Our CAV silencing does not selectively infect TM cells, so a portion of the outflow effect observed could also be contributed by altered CAV function in SC inner wall cells.

Recent data indicate that global *CAV1* knockout mice had significantly increased IOPs at 12 to 24 weeks compared with age- and sex-matched wild-type littermates (Elliott MH, et al. *IOVS* 2014; 55:ARVO E-Abstract 2888). This data appear to be directly opposite to the effects we have described in *CAV1*-silenced human and porcine perfused cultures. However, multiple factors may influence the results of each of our studies. Our silencing studies reduce, but do not completely eliminate CAV1 protein. Thus, a small amount of CAV1 may still function as normal and be available to interact with CAV2. In knockout mice, these functions and/or interactions would be completely eliminated. In the absence of CAV1, CAV2 is trapped at the Golgi, where it is targeted to the proteasomal degradation pathway.[20,25,26] Our perfusion studies show that knockdown of *CAV2* decreases outflow rate, which correlates to increased IOP. Consequently, the data from both studies

may not be contrary, but rather the increased IOP in the CAV1 null mouse may be due to concomitant mislocalization and proteasomal degradation of CAV2. Although this is the most likely explanation, other factors could also play a role. Since the *CAV1* mouse was a global knockout, it remains possible that other factors also contributed, including alterations in aqueous humor production, central corneal thickness, or there may be a decrease in alternative pathway outflow, which accounts for a much higher (80%) amount of aqueous flow in mouse eyes than in human eyes. These factors could all influence IOP either separately, or in combination. In addition, chronic loss of *CAV1* in mice may also affect ECM turnover differently than a transient loss of CAV1 function by silencing, which could contribute to the observed outflow differences. Chronic alterations in turnover can lead to excessive accumulation of ECM components and decreased elasticity of the tissue as evidenced by fibrotic scar tissue. Certainly, glaucomatous TMs show an accumulation of ECM, increased stiffness of the tissue and increased IOP.[59,60] More studies both with our knockdown perfusion system and with the *CAV1* knockout mouse model are required in order to investigate the mechanism of CAV1 function in the aqueous humor pathway.

There are other potential ways that CAV knockdown could influence outflow. Endothelial nitric oxide synthase (eNOS) interacts with the scaffolding domain of CAV1 in caveolae, which maintains eNOS in an inactive state.[61] This suggests that in the absence of CAV1, there is increased activation and release of eNOS (Elliott MH, et al. *IOVS* 2014; 55:ARVO E-Abstract 2888). Certainly, overexpression of eNOS in transgenic mice lowered IOP by increasing aqueous drainage through the conventional pressure-dependent outflow pathway.[62] This lowering of IOP is consistent with the increase in outflow rate found in *CAV1*-silenced perfused anterior segments.

This is the first study to implicate caveolins in the regulation of ADAMTS4 activity. A highly homologous ADAMTS, ADAMTS5, was found endocytosed by low-density lipoprotein receptor–related protein-1 (LRP-1) in cartilage chondrocytes.[63] Application of a specific LRP-1 endocytosis inhibitor increased ADAMTS5-mediated ECM degradation showing that endocytosis functionally regulates ADAMTS activity. In this study, we showed that ADAMTS4 activity was increased in CAV-silenced TM cells by two methods: an increase in activity was observed using a quenched fluorogenic peptide substrate assay and there was an increase in the appearance of the neoepitope of versican, a substrate for ADAMTS4. Moreover, both ADAMTS4 and the versican neoepitope antibodies colocalized with endogenous CAV1 and CAV2 in TM cells. Thus, caveolin-mediated endocytosis appears to regulate ADAMTS4 activity in the ECM. However, this does not exclude the possibility that other endocytic pathways are also involved in the regulation of not only ADAMTS4, but also the MMPs. Further studies are required to evaluate the contributions of clathrin, flotillin, and LRP-1 endocytic pathways in regulating ECM turnover in the TM.

There was a significant increase in fibronectin protein levels in response to *CAV* silencing in cells and tissue. While it is well known that turnover of fibronectin involves CAV1-mediated endocytosis and intracellular degradation,[33] this is the first report suggesting that CAV2 also affects fibronectin turnover. Since fibronectin levels were increased when silencing either of the CAVs, but the effects of CAV silencing on outflow were opposite, it seems unlikely that fibronectin itself is responsible for the outflow resistance. However, fibronectin is known to orchestrate the deposition and maintenance of other ECM molecules, including tenascin C, collagen types I and III, and thrombospondin-1.[64–66] Furthermore, fibronectin polymerization is a potent inhibitor of integrin endocytosis.[30] Therefore, the increase in fibronectin due to a reduction in *CAV1* or *CAV2* levels could profoundly influence the composition and organization of the ECM in the outflow channels in the TM. We hypothesize that differences in the organization of the resistance components by fibronectin could contribute to the opposite effects on outflow.

Increased fibronectin levels have also been linked to increased ECM rigidity.[31] A stiffer ECM profoundly influences mechanotransduction. For instance, a previous study (Elliott MH, et al. *IOVS* 2014; 55:ARVO E-Abstract 2888) showed that stress fibers were prevalent in TM cells when they were cultured on stiff matrices and that αSMA expression was increased when cultured on rigid structures.[67] In this study, we show an increased appearance of actin stress fibers and αSMA expression in *CAV* knockdown cells. Alterations in these cytoskeletal components could also contribute to the observed differences in outflow facility since cytoskeletal manipulators alter TM cell contractility and outflow rates are concomitantly changed in perfusion culture and in animal models.[68]

One caveat of this study is that both CAV1 and CAV2 have multiple alternative isoforms. Our silencing constructs target both of the known CAV1 isoforms, but only three of the four CAV2 isoforms. Caveolin 2 isoform c, which lacks exon 3, is not targeted by our silencing construct. In other cell types, this CAV2 isoform appeared to be expressed at much lower levels than full-length CAV2 and was immunolocalized to the endoplasmic reticulum instead of the Golgi or plasma membrane.[69] The significance and expression levels of these CAV isoforms in TM cells and outflow resistance requires further analysis.

In conclusion, our study shows altered MMP/ADAMTS4 activity and ECM protein levels in response to *CAV1* and *CAV2* silencing. Moreover, application of sh*CAV1* and sh*CAV2* to perfusion culture revealed a significant, but opposite effect on outflow. Caveolin-mediated endocytosis is one mechanism by which TM cells can dictate the physiological catabolism of ECM in the TM in order to alter outflow resistance. Dysregulation of CAV function in the TM could contribute to the pathological changes in ECM that is observed in glaucoma.

Acknowledgments

We thank Ruth Phinney at Lions Eye bank, Portland, Oregon, for aiding in the procurement of human eyes and Aurelie Snyder at the Advanced Light Microscopy core facility of OHSU for assisting in the calculation of the Pearson's correlation coefficients.

Supported by NIH/National Eye Institute Grants EY019643 (KEK); EY003279, EY008247, EY010572 (TSA); the Sybil B. Harrington Special Scholar Award from Research to Prevent Blindness (KEK); and an unrestricted grant to the Casey Eye Institute by Research to Prevent Blindness.

Disclosure: **M. Aga**, None; **J.M. Bradley**, None; **R. Wanchu**, None; **Y.-F. Yang**, None; **T.S. Acott**, None; **K.E. Keller**, None

References

1. Boland MV, Quigley HA. Risk factors and open-angle glaucoma: classification and application. *J Glaucoma*. 2007;16:406–418.
2. Rezaie T, Child A, Hitchings R, et al. Adult-onset primary open-angle glaucoma caused by mutations in optineurin. *Science*. 2002;295:1077–1079.
3. Stone EM, Fingert JH, Alward WL, et al. Identification of a gene that causes primary open angle glaucoma. *Science*. 1997;275:668–670.
4. Monemi S, Spaeth G, DaSilva A, et al. Identification of a novel adult-onset primary open-angle glaucoma (POAG) gene on 5q22.1. *Hum Mol Genet*. 2005;14:725–733.

5. Pasutto F, Keller KE, Weisschuh N, et al. Variants in ASB10 are associated with open-angle glaucoma. *Hum Mol Genet*. 2012; 21:1336–1349.
6. Allingham RR, Liu Y, Rhee DJ. The genetics of primary open-angle glaucoma: a review. *Exp Eye Res*. 2009;88:837–844.
7. Burdon KP, Macgregor S, Hewitt AW, et al. Genome-wide association study identifies susceptibility loci for open angle glaucoma at TMCO1 and CDKN2B-AS1. *Nat Genet*. 2011;43: 574–578.
8. Pasutto F, Matsumoto T, Mardin CY, et al. Heterozygous NTF4 mutations impairing neurotrophin-4 signaling in patients with primary open-angle glaucoma. *Am J Hum Genet*. 2009;85: 447–456.
9. Pasutto F, Chavarria-Soley G, Mardin CY, et al. Heterozygous loss-of-function variants in CYP1B1 predispose to primary open-angle glaucoma. *Invest Ophthalmol Vis Sci*. 2010;51: 249–254.
10. Thorleifsson G, Walters GB, Hewitt AW, et al. Common variants near CAV1 and CAV2 are associated with primary open-angle glaucoma. *Nat Genet*. 2010;42:906–909.
11. Wiggs JL, Kang JH, Yaspan BL, et al. Common variants near CAV1 and CAV2 are associated with primary open-angle glaucoma in Caucasians from the USA. *Hum Mol Genet*. 2011; 20:4707–4713.
12. Kuehn MH, Wang K, Roos B, et al. Chromosome 7q31 POAG locus: ocular expression of caveolins and lack of association with POAG in a US cohort. *Mol Vis*. 2011;17:430–435.
13. Abu-Amero KK, Kondkar AA, Mousa A, Osman EA, Al-Obeidan SA. Lack of association of SNP rs4236601 near CAV1 and CAV2 with POAG in a Saudi cohort. *Mol Vis*. 2012;18:1960–1965.
14. Huang W, Wang W, Zhou M, Zhang X. Association of single-nucleotide polymorphism rs4236601 near caveolin 1 and 2 with primary open-angle glaucoma: a meta-analysis [published online ahead of print October 8, 2013]. *Clin Exp Ophthalmol*. doi:10.1111/ceo.12201.
15. Fujimoto T, Kogo H, Nomura R, Une T. Isoforms of caveolin-1 and caveolar structure. *J Cell Sci*. 2000;113(pt 19):3509–3517.
16. Parton RG, Simons K. The multiple faces of caveolae. *Nat Rev Mol Cell Biol*. 2007;8:185–194.
17. Scherer PE, Okamoto T, Chun M, Nishimoto I, Lodish HF, Lisanti MP. Identification, sequence, and expression of caveolin-2 defines a caveolin gene family. *Proc Natl Acad Sci U S A*. 1996;93:131–135.
18. Scherer PE, Lewis RY, Volonte D, et al. Cell-type and tissue-specific expression of caveolin-2. Caveolins 1 and 2 co-localize and form a stable hetero-oligomeric complex in vivo. *J Biol Chem*. 1997;272:29337–29346.
19. Kwon H, Lee J, Jeong K, Jang D, Pak Y. A novel actin cytoskeleton-dependent noncaveolar microdomain composed of homo-oligomeric caveolin-2 for activation of insulin signaling. *Biochim Biophys Acta*. 2013;1833:2176–2189.
20. Drab M, Verkade P, Elger M, et al. Loss of caveolae, vascular dysfunction, and pulmonary defects in caveolin-1 gene-disrupted mice. *Science*. 2001;293:2449–2452.
21. Park DS, Lee H, Frank PG, et al. Caveolin-1-deficient mice show accelerated mammary gland development during pregnancy, premature lactation, and hyperactivation of the Jak-2/STAT5a signaling cascade. *Mol Biol Cell*. 2002;13:3416–3430.
22. Razani B, Combs TP, Wang XB, et al. Caveolin-1-deficient mice are lean, resistant to diet-induced obesity, and show hypertriglyceridemia with adipocyte abnormalities. *J Biol Chem*. 2002; 277:8635–8647.
23. Fra AM, Williamson E, Simons K, Parton RG. De novo formation of caveolae in lymphocytes by expression of VIP21-caveolin. *Proc Natl Acad Sci U S A*. 1995;92:8655–8659.
24. Razani B, Wang XB, Engelman JA, et al. Caveolin-2-deficient mice show evidence of severe pulmonary dysfunction without disruption of caveolae. *Mol Cell Biol*. 2002;22:2329–2344.
25. Parolini I, Sargiacomo M, Galbiati F, et al. Expression of caveolin-1 is required for the transport of caveolin-2 to the plasma membrane. Retention of caveolin-2 at the level of the Golgi complex. *J Biol Chem*. 1999;274:25718–25725.
26. Mora R, Bonilha VL, Marmorstein A, et al. Caveolin-2 localizes to the golgi complex but redistributes to plasma membrane, caveolae, and rafts when co-expressed with caveolin-1. *J Biol Chem*. 1999;274:25708–25717.
27. Zhu LL, Cui Y, Chang YS, Fang FD. A second protein marker of caveolae: caveolin-2. *Chin Med Sci J*. 2010;25:119–124.
28. Acott TS, Kelley MJ. Extracellular matrix in the trabecular meshwork. *Exp Eye Res*. 2008;86:543–561.
29. Cox TR, Erler JT. Remodeling and homeostasis of the extracellular matrix: implications for fibrotic diseases and cancer. *Dis Model Mech*. 2011;4:165–178.
30. Shi F, Sottile J. MT1-MMP regulates the turnover and endocytosis of extracellular matrix fibronectin. *J Cell Sci*. 2011;124:4039–4050.
31. Goetz JG, Minguet S, Navarro-Lerida I, et al. Biomechanical remodeling of the microenvironment by stromal caveolin-1 favors tumor invasion and metastasis. *Cell*. 2011;146:148–163.
32. Hocking DC, Kowalski K. A cryptic fragment from fibronectin's III1 module localizes to lipid rafts and stimulates cell growth and contractility. *J Cell Biol*. 2002;158:175–184.
33. Sottile J, Chandler J. Fibronectin matrix turnover occurs through a caveolin-1-dependent process. *Mol Biol Cell*. 2005; 16:757–768.
34. Chow AK, Cena J, El-Yazbi AF, et al. Caveolin-1 inhibits matrix metalloproteinase-2 activity in the heart. *J Mol Cell Cardiol*. 2007;42:896–901.
35. Kandasamy AD, Chow AK, Ali MA, Schulz R. Matrix metalloproteinase-2 and myocardial oxidative stress injury: beyond the matrix. *Cardiovasc Res*. 2010;85:413–423.
36. Cho WJ, Chow AK, Schulz R, Daniel EE. Matrix metalloproteinase-2, caveolins, focal adhesion kinase and c-Kit in cells of the mouse myocardium. *J Cell Mol Med*. 2007;11: 1069–1086.
37. Aga M, Bradley JM, Keller KE, Kelley MJ, Acott TS. Specialized podosome- or invadopodia-like structures (PILS) for focal trabecular meshwork extracellular matrix turnover. *Invest Ophthalmol Vis Sci*. 2008;49:5353–5365.
38. Webb BA, Eves R, Mak AS. Cortactin regulates podosome formation: roles of the protein interaction domains. *Exp Cell Res*. 2006;312:760–769.
39. Artym VV, Zhang Y, Seillier-Moiseiwitsch F, Yamada KM, Mueller SC. Dynamic interactions of cortactin and membrane type 1 matrix metalloproteinase at invadopodia: defining the stages of invadopodia formation and function. *Cancer Res*. 2006;66:3034–3043.
40. van den Dries K, Schwartz SL, Byars J, et al. Dual-color superresolution microscopy reveals nanoscale organization of mechanosensory podosomes. *Mol Biol Cell*. 2013;24:2112–2123.
41. Keller KE, Aga M, Bradley JM, Kelley MJ, Acott TS. Extracellular matrix turnover and outflow resistance. *Exp Eye Res*. 2009;88: 676–682.
42. Surgucheva I, Surguchov A. Expression of caveolin in trabecular meshwork cells and its possible implication in pathogenesis of primary open angle glaucoma. *Mol Vis*. 2011; 17:2878–2888.
43. Stamer WD, Seftor RE, Williams SK, Samaha HA, Snyder RW. Isolation and culture of human trabecular meshwork cells by extracellular matrix digestion. *Curr Eye Res*. 1995;14:611–617.

Investigative Ophthalmology & Visual Science

44. Polansky JR, Weinreb RN, Baxter JD, Alvarado J. Human trabecular cells. I. Establishment in tissue culture and growth characteristics. *Invest Ophthalmol Vis Sci*. 1979;18:1043–1049.
45. Keller KE, Bradley JM, Vranka JA, Acott TS. Segmental versican expression in the trabecular meshwork and involvement in outflow facility. *Invest Ophthalmol Vis Sci*. 2011;52:5049–5057.
46. Lu Z, Overby DR, Scott PA, Freddo TF, Gong H. The mechanism of increasing outflow facility by rho-kinase inhibition with Y-27632 in bovine eyes. *Exp Eye Res*. 2008;86:271–281.
47. Zinchuk V, Zinchuk O, Okada T. Quantitative colocalization analysis of multicolor confocal immunofluorescence microscopy images: pushing pixels to explore biological phenomena. *Acta Histochem Cytochem*. 2007;40:101–111.
48. Zinchuk V, Wu Y, Grossenbacher-Zinchuk O. Bridging the gap between qualitative and quantitative colocalization results in fluorescence microscopy studies. *Sci Rep*. 2013;3:1365.
49. Keller KE, Sun YY, Yang YF, Bradley JM, Acott TS. Perturbation of hyaluronan synthesis in the trabecular meshwork and the effects on outflow facility. *Invest Ophthalmol Vis Sci*. 2012;53:4616–4625.
50. Keller KE, Sun YY, Vranka JA, Hayashi L, Acott TS. Inhibition of hyaluronan synthesis reduces versican and fibronectin levels in trabecular meshwork cells. *PLoS One*. 2012;7:e48523.
51. Keller KE, Bradley JM, Kelley MJ, Acott TS. Effects of modifiers of glycosaminoglycan biosynthesis on outflow facility in perfusion culture. *Invest Ophthalmol Vis Sci*. 2008;49:2495–2505.
52. Keller KE, Bradley JM, Acott TS. Differential effects of ADAMTS-1, -4, and -5 in the trabecular meshwork. *Invest Ophthalmol Vis Sci*. 2009;50:5769–5777.
53. Martin KH, Hayes KE, Walk EL, Ammer AG, Markwell SM, Weed SA. Quantitative measurement of invadopodia-mediated extracellular matrix proteolysis in single and multicellular contexts. *J Vis Exp*. 2012;e4119.
54. Bradley JM, Vranka J, Colvis CM, et al. Effect of matrix metalloproteinases activity on outflow in perfused human organ culture. *Invest Ophthalmol Vis Sci*. 1998;39:2649–2658.
55. Hinz B. The myofibroblast: paradigm for a mechanically active cell. *J Biomech*. 2010;43:146–155.
56. Herrnberger L, Ebner K, Junglas B, Tamm ER. The role of plasmalemma vesicle-associated protein (PLVAP) in endothelial cells of Schlemm's canal and ocular capillaries. *Exp Eye Res*. 2012;105:27–33.
57. Tamm ER. The trabecular meshwork outflow pathways: structural and functional aspects. *Exp Eye Res*. 2009;88:648–655.
58. Overby DR, Stamer WD, Johnson M. The changing paradigm of outflow resistance generation: towards synergistic models of the JCT and inner wall endothelium. *Exp Eye Res*. 2009;88:656–670.
59. Tektas OY, Lutjen-Drecoll E. Structural changes of the trabecular meshwork in different kinds of glaucoma. *Exp Eye Res*. 2009;88:769–775.
60. Last JA, Pan T, Ding Y, et al. Elastic modulus determination of normal and glaucomatous human trabecular meshwork. *Invest Ophthalmol Vis Sci*. 2011;52:2147–2152.
61. Parat MO. The biology of caveolae: achievements and perspectives. *Int Rev Cell Mol Biol*. 2009;273:117–162.
62. Stamer WD, Lei Y, Boussommier-Calleja A, Overby DR, Ethier CR. eNOS, a pressure-dependent regulator of intraocular pressure. *Invest Ophthalmol Vis Sci*. 2011;52:9438–9444.
63. Yamamoto K, Troeberg L, Scilabra SD, et al. LRP-1-mediated endocytosis regulates extracellular activity of ADAMTS-5 in articular cartilage. *FASEB J*. 2013;27:511–521.
64. Sottile J, Hocking DC. Fibronectin polymerization regulates the composition and stability of extracellular matrix fibrils and cell-matrix adhesions. *Mol Biol Cell*. 2002;13:3546–3559.
65. Velling T, Risteli J, Wennerberg K, Mosher DF, Johansson S. Polymerization of type I and III collagens is dependent on fibronectin and enhanced by integrins alpha 11beta 1 and alpha 2beta 1. *J Biol Chem*. 2002;277:37377–37381.
66. Chung CY, Zardi L, Erickson HP. Binding of tenascin-C to soluble fibronectin and matrix fibrils. *J Biol Chem*. 1995;270:29012–29017.
67. Schlunck G, Han H, Wecker T, Kampik D, Meyer-ter-Vehn T, Grehn F. Substrate rigidity modulates cell matrix interactions and protein expression in human trabecular meshwork cells. *Invest Ophthalmol Vis Sci*. 2008;49:262–269.
68. Tian B, Gabelt BT, Geiger B, Kaufman PL. The role of the actomyosin system in regulating trabecular fluid outflow. *Exp Eye Res*. 2009;88:713–717.
69. Kogo H, Ishiguro K, Kuwaki S, Fujimoto T. Identification of a splice variant of mouse caveolin-2 mRNA encoding an isoform lacking the C-terminal domain. *Arch Biochem Biophys*. 2002;401:108–114.

Investigative Ophthalmology & Visual Science